

Variation in entrainment rate and relationship with cloud microphysical properties on the scale of 5 m

Muning Cheng · Chunsong Lu · Yangang Liu

Received: 11 November 2014 / Accepted: 25 December 2014 / Published online: 3 February 2015
© Science China Press and Springer-Verlag Berlin Heidelberg 2015

Abstract This paper focuses on the variability in entrainment rate in individual cumulus clouds using the entrainment rate estimated on the scale of 5 m in 186 shallow cumulus clouds from eight aircraft flights, using in situ observations from the RACORO field campaign (the routine atmospheric radiation measurement aerial facility clouds with low optical water depths optical radiative observations) over the atmospheric radiation measurement Southern Great Plains site, USA. The result shows that the mean entrainment rate of all the 186 clouds systematically decreases from the cloud edge to the cloud center. Further analysis of the fluctuation of entrainment rate shows that the probability density function of entrainment rate in each

flight can be fitted by the lognormal, gamma, or Weibull distributions virtually equally well, with the Weibull distribution being the best. The parameter “standard deviation” in the lognormal distribution is weakly negatively correlated, and the other parameters in the three distributions are positively correlated with relative humidity in the entrained dry air and dilution effect, respectively. Entrainment rate is negatively correlated with droplet concentration, droplet size, and liquid water content, but positively correlated with relative dispersion. The effect of entrainment rate on the spectral shape of cloud droplet size distribution is examined and linked to the systems theory on the cloud droplet size distribution.

Electronic supplementary material The online version of this article (doi:10.1007/s11434-015-0737-8) contains supplementary material, which is available to authorized users.

Keywords Entrainment rate · Shallow cumulus · Aircraft observations · Probability density functions · Microphysics

M. Cheng
Jiangsu Provincial Key Laboratory of Environmental Engineering, Jiangsu Provincial Academy of Environmental Science, Nanjing 210036, China

M. Cheng · C. Lu
State Key Laboratory of Severe Weather, Chinese Academy of Meteorological Sciences, Beijing 100081, China

C. Lu (✉)
Collaborative Innovation Center on Forecast and Evaluation of Meteorological Disasters, Key Laboratory for Aerosol-Cloud-Precipitation of China Meteorological Administration, Key Laboratory of Meteorological Disaster of Ministry of Education, Nanjing University of Information Science and Technology, Nanjing 210044, China
e-mail: clu@nuist.edu.cn

Y. Liu
Biological, Environmental and Climate Science Department, Brookhaven National Laboratory, Upton, NY 11973, USA

1 Introduction

Clouds play important roles in global radiation budget and climate change [1–7]. Cumulus parameterization in climate models affects the simulations of precipitation, intraseasonal oscillation, and climate [8–12]. Fractional entrainment rate (λ) is an important property widely used in the parameterization of cumulus clouds and has been known to influence the transport of heat, momentum, and water vapor [13, 14]. Entrainment and the subsequent mixing processes significantly affects cloud properties [15–18].

In the past several decades, a number of approaches have been developed to estimate entrainment rate. Stommel [19] calculated the entrainment rate from moisture and temperature profiles inside and outside of clouds and found that the amount of entrained dry air was about twice the

original cloudy air. Betts [20] developed a bulk-plume approach, whereby entrainment rate was estimated from the difference in a conserved property between cloud and environment. Later on, this approach was used to estimate entrainment rate from model simulations [21, 22] and observations [23–25]. These results indicated that entrainment rate was different for different clouds. For example, de Rooy and Siebesma [21] found entrainment rate decreased with height while Del Genio and Wu [22] found an opposite phenomenon. Jensen and Del Genio [26] estimated entrainment rate through comparing cloud-top height from an entraining parcel model with that from observations. They found that, on average, entrainment rate was approximately constant for low cloud-top height and entrainment rate decreased with further increasing cloud-top height. Wagner et al. [27] developed an algorithm for estimating entrainment rate based on a mixing parcel model and ground-based observations. They found that shallow cumulus clouds showed significant variability in entrainment rate in a single day and from one day to the next. Romps [28] introduced a method for directly measuring entrainment rate in a cloud-resolving simulation. It was found that the bulk-plume method underestimates entrainment rate by roughly a factor of 2. Dawe and Austin [29] formulated a method for estimating entrainment rate through the surface of an arbitrary volume in a numerical model. They further applied this method to large eddy simulations and found that entrainment rate was best predicted by mean cloud buoyancy and environmental buoyancy lapse rate [30]. Despite the effort and progress, the topic is still poorly understood and entrainment rate reported in the literature continues to suffer from a large uncertainty [24, 31, 32].

Furthermore, entrainment-mixing can be treated as a stochastic process, and probability density function (PDF) of entrainment rate is important to improve cumulus parameterizations [33, 34]. Unfortunately, observational studies on the PDF of entrainment rate are rare. Lately, Lu et al. [35] studied cloud-mean entrainment rate for 186 growing cumulus clouds based on aircraft observations and examined PDF of entrainment rate. However, in that study, only cloud-mean entrainment rate was investigated. It is desirable to know the spatial variation and statistics of entrainment rate within individual clouds because entrainment-mixing is a local phenomenon and is expected to vary within individual clouds. To the best of our knowledge, there have been no observational studies on the spatial variation and PDF of entrainment rate in individual clouds on a scale smaller than cloud itself. Likewise, the effects of entrainment rate on cloud microphysical properties have been hardly examined on a sub-cloud scale.

The objective of this work was to fill these gaps using the 5-m-resolution data collected during the Routine AAF

[atmospheric radiation measurement (ARM) aerial facility] clouds with low optical water depths (CLOWD) optical radiative observations (RACORO) field campaign, which operated over the ARM Southern Great Plains (SGP) site near Lamont, Oklahoma, US, from January 22 to June 30, 2009 [36, 37]. We investigate the spatial variability and PDF of entrainment rate, and the relationship between entrainment rate and cloud microphysical properties on the scale of 5 m.

2 Observational data and approach

2.1 Observational data

The same dataset from RACORO in Lu et al. [35, 38] is analyzed here. A total of 186 growing cumulus clouds in eight flights (May 22, May 23, May 24, June 11, June 19, June 23, June 24, and June 26, 2009) [36] are examined. Comprehensive measurements of radiation, cloud, atmospheric state parameters, and aerosol were made by the Twin Otter aircraft from the Center for Interdisciplinary Remotely Piloted Aircraft Studies (CIRPAS). Cloud droplet size distributions were measured by Cloud and Aerosol Spectrometer (CAS) at a sampling rate of 10 Hz. The CAS probe measures aerosol particles and cloud droplets from 0.29 to 25 μm (20 bins in radius). Only the bins with a bin-averaged radius larger than 1 μm are employed to calculate cloud microphysical quantities. The criteria of number concentration (n) $> 10 \text{ cm}^{-3}$ and liquid water content (LWC) $> 0.001 \text{ g m}^{-3}$ are employed to select cloud droplet size distributions [39]. According to Baumgardner et al. [40], the CAS probe has a time response of 0.1 μs and utilizes a first-in, first-out buffer that eliminates any dead time losses until number concentration exceeds $13,000 \text{ cm}^{-3}$. Thus, the CAS probe is fast enough to measure cloud droplet size distributions at the aircraft speed of 50 m s^{-1} . Furthermore, the sampling area of the CAS is $11.1 \text{ mm} \times 120 \mu\text{m}$, so the sampling volume at 10 Hz is $11.1 \text{ mm} \times 120 \mu\text{m} \times 50 \text{ m s}^{-1} \times 0.1 \text{ s}$, i.e., 6.66 cm^{-3} . The number concentration in this study is mainly on the order of 100 cm^{-3} . Assume that the number concentration is 100 cm^{-3} , the number of droplets in the sampling volume is 666. Even for the number concentration threshold in this study, 10 cm^{-3} , the number of droplets in the sampling volume is 66.6. Thus, the observations of each cloud droplet size distributions and microphysical properties should be reliable based on a large number of droplets. The cloud imaging probe (CIP) measured droplets in the range of 7.50 to 781 μm (radius) at a sampling rate of 1 Hz. The criterion that the in-cloud mean drizzle LWC (radius $> 25 \mu\text{m}$ from the CIP) over the observation period smaller than 0.005 g m^{-3} is used to identify non-drizzling clouds. Water vapor and temperature were measured at 10 Hz, respectively, with Diode Laser

Hygrometer (DLH) and a Rosemount probe [41, 42]. Vertical velocity was measured with a 5-hole gust probe on the nose of the aircraft.

Individual growing cumulus clouds are identified based on the criteria: (1) when the distance between two CAS cloud droplet size distributions is less than 50 m, they are considered to be within the same cumulus cloud (the data were collected on the scale of 5 m because of the 10-Hz CAS sampling rate and the aircraft speed of 50 m s⁻¹); (2) 80 % of vertical velocity in an individual cloud is positive [25, 43]; (3) cloud has more than 30 cloud droplet size distributions. Only the entrainment rate in cloud cores is estimated here. The edge of the cloud core is defined as the point where vertical velocity changes from negative to positive for the first time, along the direction from the cloud edge toward the interior of the cloud (see Fig. 1a in Lu et al. [35] for details). Lu et al. [35] examined the dependence of calculated entrainment rate on the above arbitrary thresholds for selecting growing clouds and found that the effects of these thresholds were minor.

2.2 Approach

The approach for estimating entrainment rate was described by Lu et al. [43]. As shown in Fig. 1, aircraft penetrates clouds at the height of z , collecting cloud data at a spatial resolution of 5 m. It is assumed that each cloud droplet size distribution corresponds to a 5-m-long cloud parcel and a cloud core is composed of tens or hundreds of cloud parcels. Assume that all these cloud parcels grow adiabatically from the cloud base to the level of z . Dry air at that level is assumed to be entrained into each adiabatic cloud parcel; after mixing and evaporation, adiabatic liquid water mixing ratio in each cloud parcel decreases to the observed liquid water mixing ratio.

Two quantities are needed to estimate entrainment rate. The first one is the mixing fraction of adiabatic cloud (χ),

which can be calculated based on the conservations of total water and energy during the entrainment-mixing at z ; the same method was widely used in other studies [25, 44–46]. See the Electronic Supplementary Material for details. The quantities needed for the calculation of χ are $q_{L,a}$, q_L , $q_{vs}(T_a)$, q_{ve} , and T_e . The $q_{L,a}$ is derived from the adiabatic liquid water content (LWC_a), which is assumed to be the maximum LWC measured in an individual cloud. q_L is mean liquid water mixing ratio in each cloud. $q_{vs}(T_a)$ is the water vapor mixing ratio at the point of LWC_a and is measured with DLH, and T_a is calculated from $q_{vs}(T_a)$ under the assumption of saturated cloud air. q_{ve} and T_e are, respectively, water vapor mixing ratio and temperature of the entrained dry air.

The second quantity needed to calculate entrainment rate is the height (h) of penetration level (z) above the cloud base height (z_0): $h = z - z_0$. The cloud base height z_0 is estimated by adiabatically moving the cloud parcel with LWC_a from the measurement level downwards and z_0 is the height where LWC_a = 0. With χ and h , entrainment rate is calculated by [43]

$$\lambda = \frac{-\ln \chi}{h} \tag{1}$$

The entrained mass is assumed to be distributed at the mid-level (h_m) above z_0 :

$$h_m = \frac{z - z_0}{2} \tag{2}$$

A sensitivity test in Lu et al. [35, 38] by assuming LWC_a was 1.25 times the maximum LWC showed that the uncertainty in entrainment rate due to the uncertainty in LWC_a was small, because of some cancelation between the numerator and denominator in Eq. (1).

Similar to Lu et al. [35, 38], dry air is assumed to be entrained from the distance ranging from D to $2D$ from the edge of a cloud core on both sides along a horizontal penetration (Lu et al. [35] for more explanations on D).

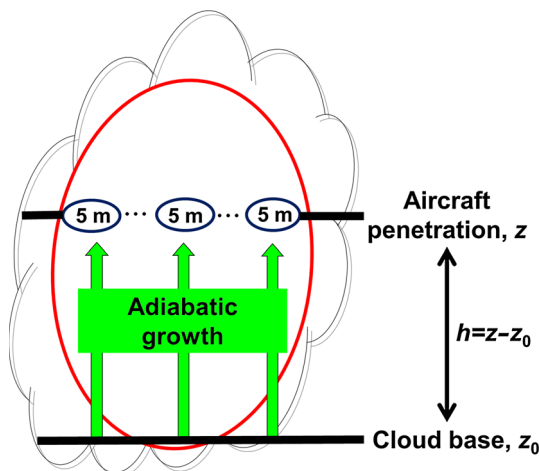


Fig. 1 (Color online) Schematic diagram of the mixing fraction approach used to estimate entrainment rate for the scale of 5 m

3 Results

3.1 Dependence of entrainment rate on distance from cloud edges

Entrainment rate is estimated for each 5-m-cloud droplet size distribution in 186 growing cumulus clouds of eight flights during RACORO. The mean entrainment rate is 0.84 km⁻¹, and the 5 %, 50 %, and 95 % percentiles are 0.07, 0.58, and 2.5 km⁻¹, respectively. The entrainment rates are comparable to the results estimated from large eddy simulations [21] and from remote sensing data [27].

As discussed in Sect. 1, it is important to study the spatial variation in entrainment rate in individual clouds on a scale

smaller than cloud itself. Here, only entrainment rates estimated for $D = 500$ m are shown because using the other D values (10, 20, 30, 40, 50, 100, and 300 m) does not affect the conclusions drawn in this study. Figure 2a shows entrainment rate as a function of normalized cloud core width for all the 186 clouds. Note that in this figure, “ $x = 0$ ” represents the cloud core centers and “ $x = \pm 0.5$ ” represents the cloud core left and right edges, respectively. As shown in Fig. 3, the cloud core width, estimated by multiplying the aircraft speed ($\sim 50 \text{ m s}^{-1}$) and the time for penetrating a cloud core, has a wide range of values with the mean core width and standard deviation being 416 and 258 m, respectively. The PDF has a peak at ~ 200 m and is skewed to the left. For majority of clouds, probability density decreases with increasing cloud core width. This result is consistent with previous observations [47]. It is clear that the mean entrainment rate decreases from the cloud core edge to the cloud center. The standard deviation of entrainment rate exhibits a similar trend, but the trend is not as significant as the mean entrainment rate itself.

The above analyses combine all the data from different heights, because the aircraft horizontal penetrations had different heights above cloud bases in different clouds. As

pointed out by many previous studies, cloud microphysics [4, 48, 49] and entrainment rate [24, 28] have significant vertical variations. Thus, it is important to examine the entrainment rate variation in individual clouds at different height levels. Here, h_m from Eq. (2) is used instead of h . As shown in Fig. 2b–d, entrainment rate also decreases from the cloud core edges to the cloud core centers even for different ranges of heights above cloud bases ($h_m = 0\text{--}50, 50\text{--}100, 100\text{--}550$ m).

The above variation in entrainment rate inside clouds is consistent with the expectation that dry air dilution decreases from cloud edges to cloud centers. This expectation is further confirmed by Fig. 4, in which the dilution effect is measured by “ 1-LWC/LWC_a .” The dilution factor 1-LWC/LWC_a decreases from the cloud core edge to the cloud center, and there is a positive correlation between entrainment rate and 1-LWC/LWC_a .

3.2 Optimal functions for describing the PDF of entrainment rate

Lu et al. [35] found that PDF of cloud-mean entrainment rate in the 186 clouds can be well fitted by the lognormal distribution. The 5-m-resolution entrainment rate data provide an

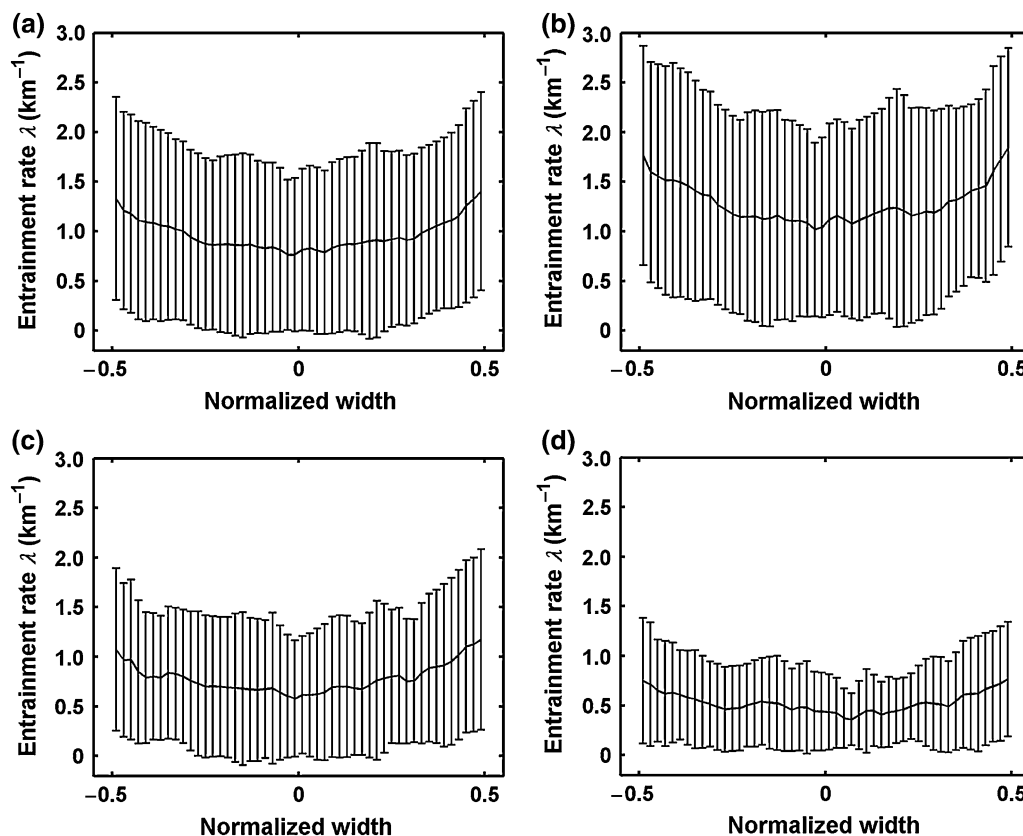


Fig. 2 Entrainment rate (λ) as a function of normalized cloud core width in the eight cumulus flights during RACORO for different ranges of height above cloud base: **a** all heights, $h_m = 0\text{--}550$ m, **b** $h_m = 0\text{--}50$ m, **c** $h_m = 50\text{--}100$ m and **d** $h_m = 100\text{--}550$ m. h_m is defined in Eq. (2). The bars represent standard deviations of entrainment rate

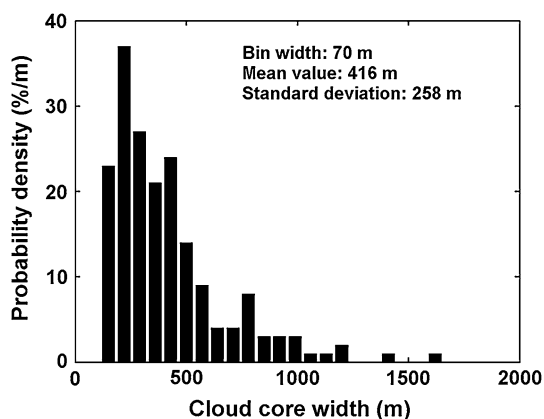


Fig. 3 Probability density function of cloud core width in the eight cumulus flights during RACORO

opportunity to study the PDF of entrainment rate in individual clouds. Most flights sampled more than 15 clouds and 1,000 cloud droplet size distributions. In one flight (June 23, 2009), there are five clouds, but they have 262 cloud droplet size distributions, still statistically significant. In addition to the lognormal distribution, this study further explores whether or not the other commonly used PDF functions, gamma and Weibull, can describe the observed PDF of entrainment rate (Table 1 summarizes the three PDF distributions and the key associated parameters). Figure 5 compares all the PDFs fitted with the three commonly used PDF distributions. It is interesting to note that the three distributions describe the observations virtually equally well, with the coefficients of determination (R^2) ranging between 0.83 and 0.98 for lognormal distribution, between 0.91 and 0.98 for gamma distribution, and between 0.91 and 0.98 for Weibull distribution.

The R^2 metric is for an individual PDF; however, one also often needs to know which distribution function (lognormal, gamma, and Weibull) is the best to fit a family of the observed PDFs. Liu et al. [50] developed such an approach based on the relationship between skewness (s) and relative dispersion (d) of the PDFs. Briefly, for the lognormal and gamma distributions, the relationships between s and d are

$$s = d^3 + 3d, \tag{3}$$

$$s = 2d, \tag{4}$$

respectively. For the Weibull distribution, s and d are uniquely related to each other, but the relationship cannot be expressed in an analytical form. Instead, s and d are given by

$$s = \frac{3q^2\Gamma(3/q) - 6q\Gamma(1/q)\Gamma(2/q) + 2\Gamma^3(1/q)}{[2q\Gamma(2/q) - \Gamma^2(1/q)]^{3/2}}, \tag{5}$$

$$d = \left[\frac{2q\Gamma(2/q)}{\Gamma^2(1/q)} - 1 \right]^{1/2}, \tag{6}$$

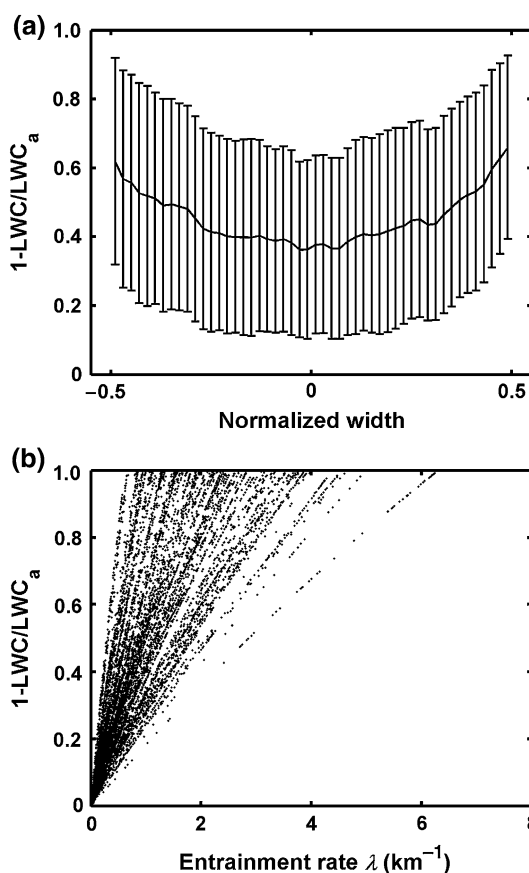


Fig. 4 a $1-LWC/LWC_a$ as a function of normalized cloud width and b entrainment rate (λ) in the eight cumulus flights during RACORO. LWC and LWC_a are liquid water content and adiabatic liquid water content in individual clouds, respectively. The bars represent standard deviations of $1-LWC/LWC_a$

respectively. Figure 6a shows the theoretical relationships between s and d from the three distributions and the results from the PDFs of entrainment rate in each flight for different D values (10, 20, 30, 40, 50, 100, 300, and 500 m). Note that on this d - s diagram, each point represents an individual PDF, whereas the different curves correspond to the different family of PDFs. The distance of the measurement points to the theoretical curves can be thus used to determine which distribution function fits the PDFs the best. It is evident from the figure

Table 1 Three PDFs for entrainment rate (λ)

Name	Formula	Parameters
Lognormal	$f(\lambda) = \frac{1}{\lambda\sigma\sqrt{2\pi}} e^{-\frac{(\ln\lambda-\mu)^2}{2\sigma^2}}$	μ and σ are mean value and standard deviation of $\ln(\lambda)$, respectively
Gamma	$f(\lambda) = \frac{1}{b^a\Gamma(a)} \lambda^{a-1} e^{-\lambda/b}$	a and b are shape and scale parameters, respectively
Weibull	$f(\lambda) = \frac{q}{c} \left(\frac{\lambda}{c}\right)^{q-1} e^{-(\lambda/c)^q}$	c and q are scale and shape parameters, respectively

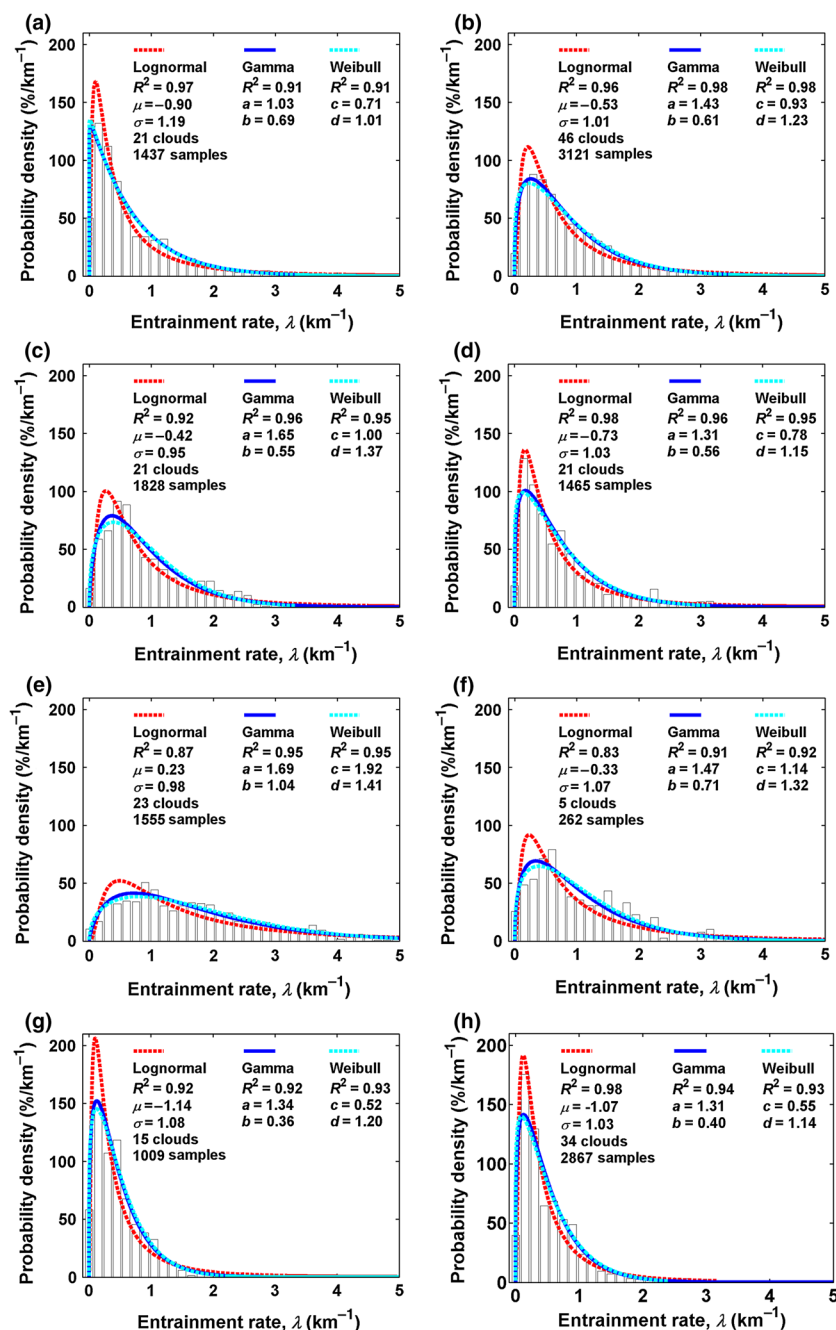


Fig. 5 Probability density functions of entrainment rate (λ) for each cumulus flight during RACORO: **a** May 22, 2009, **b** May 23, 2009, **c** May 24, 2009, **d** June 11, 2009, **e** June 19, 2009, **f** June 23, 2009, **g** June 24, 2009, and **h** June 26, 2009. The λ bin width for the PDFs is 0.15 km^{-1} . Each panel provides the coefficient of determination (R^2), the mean (μ), and standard deviation (σ) of $\ln(\lambda)$ for the lognormal fit, numbers of clouds, and 5-m entrainment rate samples in each flight; also provided are the R^2 , the shape parameter (a), scale parameter (b) for the gamma fit, and the R^2 , the scale parameter (c), shape parameter (d) for the Weibull fit

that the data points from the observed PDFs fall the closest to the line for Weibull distribution on average, suggesting that Weibull distribution is better than lognormal and gamma distributions to describe the family of PDFs of entrainment rate on the scale of 5 m in each flight. However, it is interesting to note that if using the cloud-mean entrainment rate

calculated in Lu et al. [35], the points appear to fall closer to the line for lognormal distribution (Fig. 6b). The difference in the best theoretical distribution for fitting PDFs of 5-m entrainment rate and cloud-mean entrainment rate may be related to the scale dependence of entrainment-mixing mechanisms. Data with different sampling resolutions could

result in different estimated entrainment rates. Haman et al. [51] showed that filaments of droplet-free and cloudy air were ubiquitous in clouds. A cloud sample of droplet size distribution at a lower sampling frequency (e.g., 100 m) is expected to have more droplet-free filaments than that at a higher sampling frequency (e.g., 5 m). As a result, LWC could be smaller at a lower sampling frequency, which further causes smaller χ and λ .

For the application of developing a PDF parameterization, we further estimate the parameters in the three distribution functions (μ and σ in lognormal distributions, a and b in gamma distributions, and c and q in Weibull distributions) and examine the factors that affect these parameters. As shown in Fig. 7a, μ increases with increasing mean relative humidity in the dry air of the eight flights. When relative humidity is larger, evaporation is weaker and more dry air needs to be entrained into clouds for the same decrease in LWC; so the calculated entrainment rate is larger if dry air with larger relative humidity is assumed to be entrained. This is consistent with the conclusion in Lu et al. [35] that both entrainment rate and relative humidity increase with decreasing D due to the effect of humid shells around cloud cores. The result is further substantiated by Fig. 7b, which shows that μ is positively correlated with $1-LWC/LWC_a$. Different from μ , σ is weakly negatively correlated with relative humidity in dry air and $1-LWC/LWC_a$. Figure 7c and d shows that both a and b are positively correlated with relative humidity in dry air and the dilution $1-LWC/LWC_a$, respectively. Theoretically, the mean entrainment rate from the gamma distributions is the product of a and b . As explained above for μ in lognormal distributions, larger relative humidity and $1-LWC/LWC_a$ correspond to larger mean entrainment rate, and generally also larger a and b . Similar to the shape and scale parameters in gamma distributions (i.e., a and b), the shape and scale parameters in Weibull distributions (q and c) also increase with increasing relative humidity and $1-LWC/LWC_a$ (Fig. 7e, f). The behavior of σ is different from those of a and q , which is consistent with theoretical expectations in general. These three parameters are a unique function of the PDFs' relative dispersion (the ratio of the standard deviation to the mean value). σ is positively correlated with relative dispersion, while a and q are negatively correlated with relative dispersion, respectively.

3.3 Relationships between entrainment rate and microphysics

The relationships between entrainment rate and cloud microphysical properties are underexplored, especially on the scale of 5 m. Figure 8a–c shows that entrainment rate is negatively correlated with number concentration, volume-mean radius, and mean radius. As studied by Lu et al. [38] using cloud-mean entrainment rate and microphysical properties, these negative correlations are due to the dominance of

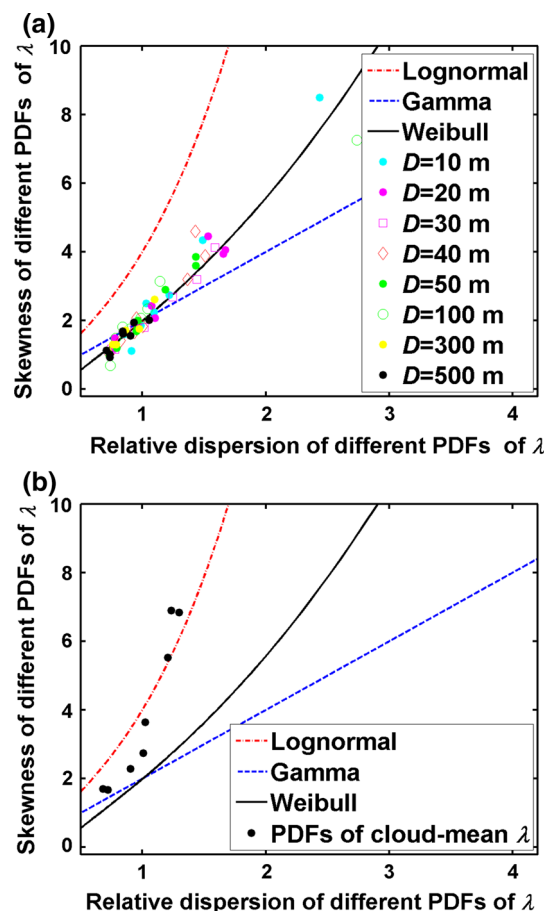


Fig. 6 **a** Skewness of probability density functions (PDFs) of entrainment rate (λ) on the scale of 5 m as a function of relative dispersion of the PDFs in each flight for different D values. The dry air is assumed to be from D to $2D$ away from the edge of the cloud core. The three lines are theoretical results for lognormal, gamma, and Weibull distributions, respectively. **b** Same as **a** but for the PDFs of cloud-mean λ from 186 cumulus clouds in eight flights. Each point corresponds to the PDF for one specific D value (10, 20, 30, 40, 50, 100, 300, and 500 m)

homogeneous entrainment-mixing mechanisms; this conclusion was also quantitatively confirmed by calculating homogeneous mixing degree [52]. The results in Fig. 8a–c indicate that the conclusion holds on the scale of 5 m. Most of standard deviations are in the range of ~ 0.75 to $\sim 1 \mu\text{m}$, and there is a positive correlation between entrainment rate and relative dispersion for the 5-m-scale data (Fig. 8d, e). The positive correlation between entrainment rate and relative dispersion is caused by a nearly constant standard deviation and a negative correlation between entrainment rate and mean radius, since relative dispersion is the ratio of standard deviation to mean radius. As shown in Fig. 8f, the negative correlation between entrainment rate and LWC arises because stronger entrainment leads to more dilution and evaporation.

To examine the effect of entrainment rate on the cloud droplet size distributions, the cloud droplet size distributions are partitioned according to the entrainment rate and

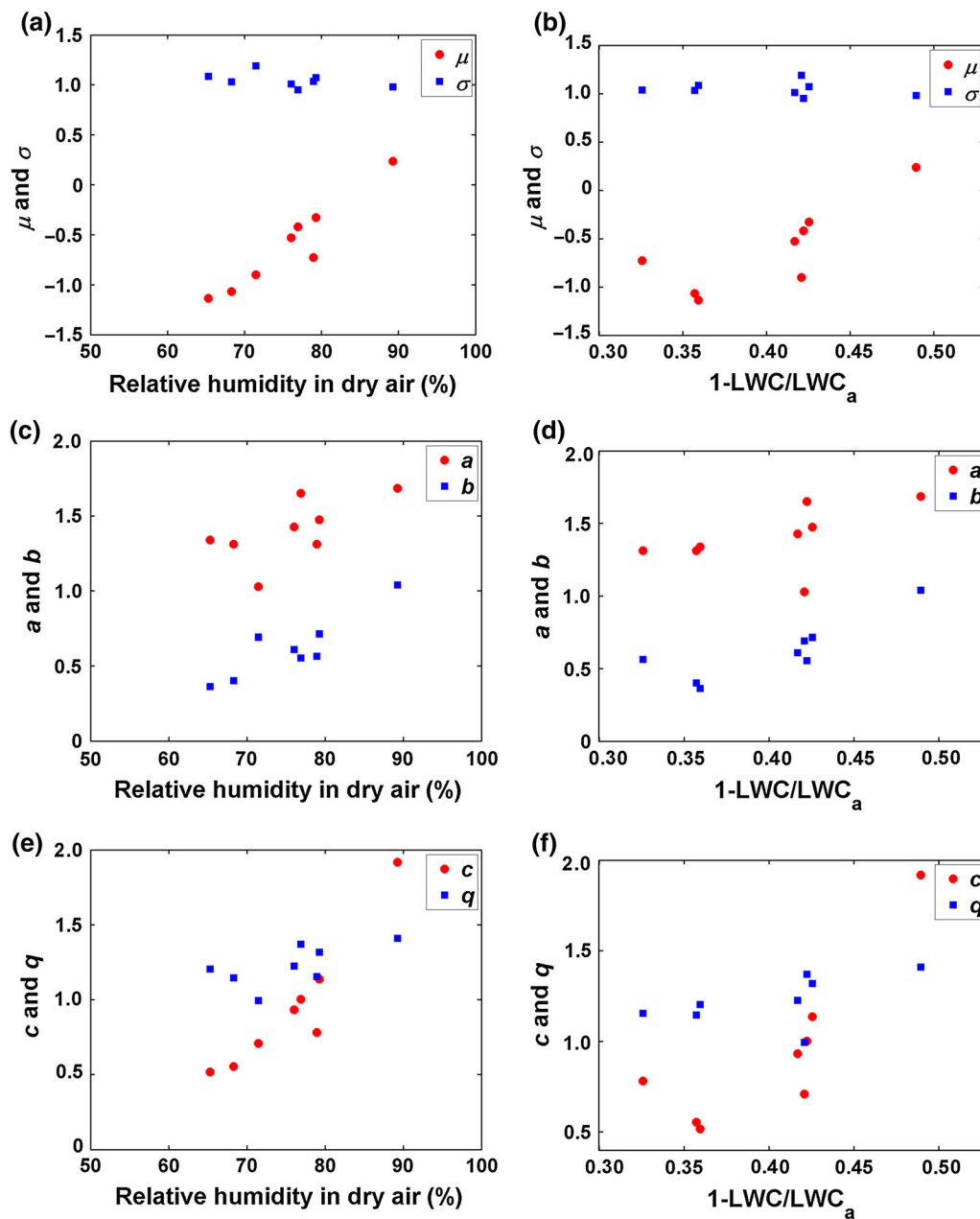


Fig. 7 (Color online) **a–b** Mean (μ) and standard deviation (σ) for the lognormal fit of probability density function of entrainment rate (λ) as a function of relative humidity in dry air and $1\text{-LWC}/\text{LWC}_a$ for each flight during RACORO, respectively. **c–d** Same as **a–b** but for the shape parameter (a) and scale parameter (b) for the gamma fit of probability density function of λ . **e–f** Same as **a–b** but for the scale parameter (c) and shape parameter (q) for the Weibull fit of probability density function of λ

plotted in a similar dispersion–skewness diagram as Fig. 6, except for the droplet size distribution instead of entrainment rate PDF (Fig. 9). It is noteworthy that when entrainment rate is smaller than 2 km^{-1} , the data points (blue) fall mainly between the lines of gamma and Weibull distributions. When entrainment rate is larger than 2 km^{-1} , the data points (cyan, yellow, and red) scatter widely from below the line of Weibull distribution to above the line of lognormal distribution. The change in the spectral shape of

the droplet size distribution with entrainment rate warrants further inspection. Liu et al. [53–57] developed a systems theory by integrating into cloud physics the ideas from statistical physics and information theory. Two conclusions derived from the systems theory are particularly relevant to the results shown in Fig. 9. First, the most probable size distribution in turbulent clouds tends to follow the Weibull distribution, which is supported by the blue points. Second, observed droplet size distributions in real clouds tend to

depend on the sampling (averaging) scale, with a saturation scale beyond which the averaged size distribution approaches the most probable Weibull distribution; clouds with stronger fluctuations tend to have larger saturation scale and higher dispersion. The difference between the observed droplet size distributions shown here and the theoretical expectation from the systems theory could be due to the data in this study may not reach the saturation scale for the

most probable size distribution. From the viewpoint of the systems theory, a stronger entrainment leads to a stronger fluctuation in clouds, which in turn leads to a larger saturation scale and stronger scale dependency of droplet size distributions [58]. This dependency on the fluctuation degree provides a qualitative explanation why the droplet size distributions deviate from the Weibull distributions significantly when entrainment rate is larger than 2 km^{-1} .

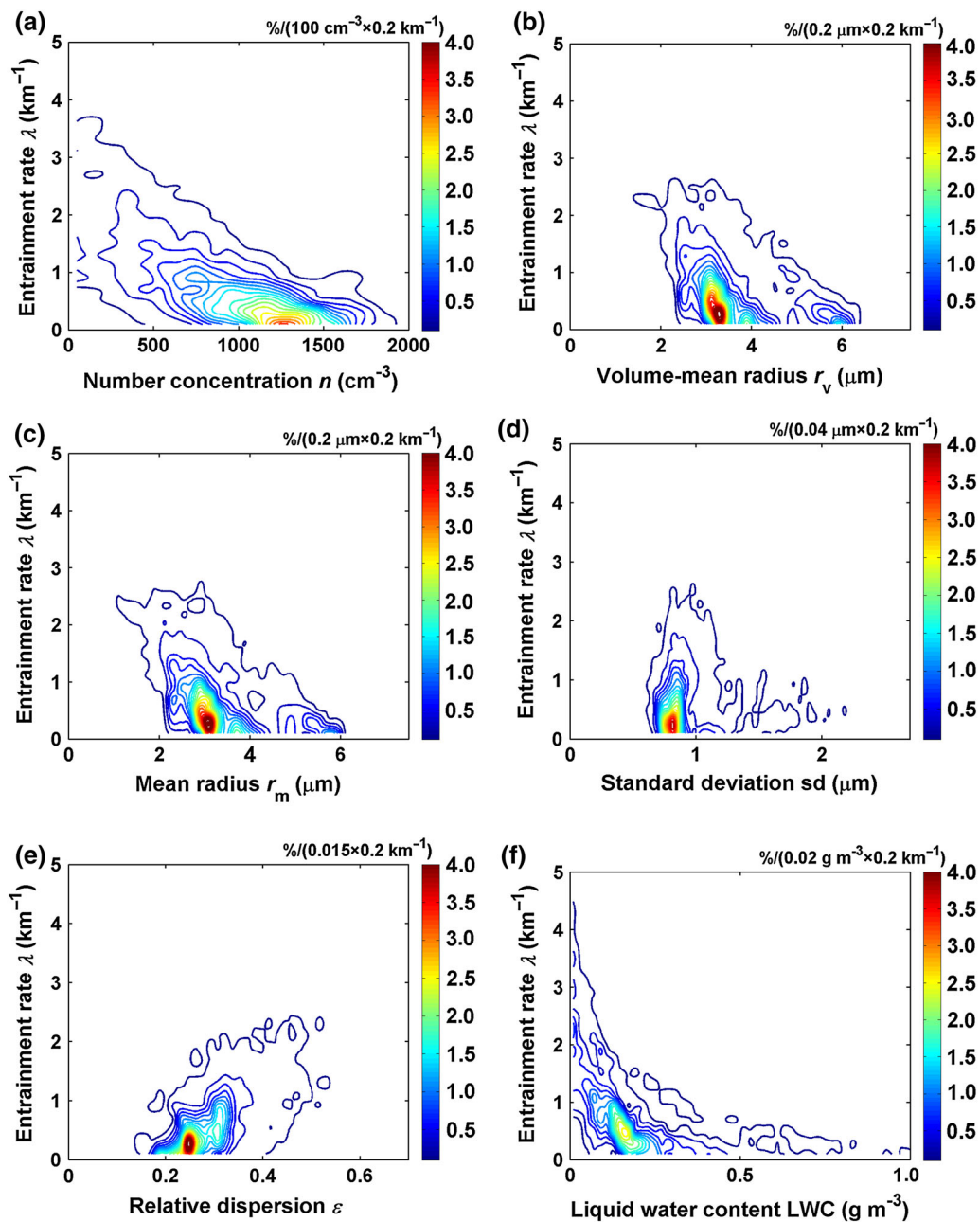


Fig. 8 Joint probability density functions of entrainment rate (λ) versus **a** number concentration (n), **b** volume-mean radius (r_v), **c** mean radius (r_m), **d** standard deviation (sd), **e** relative dispersion ($\varepsilon = sd/r_m$), and **f** liquid water content (LWC) in the eight cumulus flights during RACORO

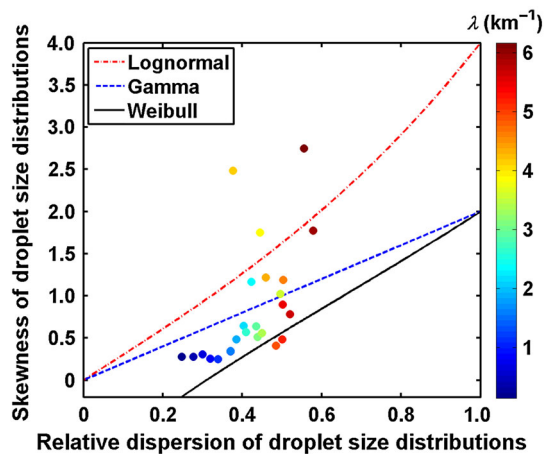


Fig. 9 Skewness of cloud droplet size distributions as a function of relative dispersion of the size distributions, which is binned according to entrainment rate (λ) in 186 growing cumulus clouds during RACORO. The three lines are theoretical results for lognormal, gamma, and Weibull distributions, respectively

4 Conclusions

Entrainment rates are estimated on the scale of 5 m using the mixing fraction approach for a total of 186 cumulus clouds collected during RACORO. The high-resolution data are examined for statistical features of the entrainment rate in individual clouds. It is found that on average, entrainment rate systematically decreases from the cloud core edge to the cloud center in the 186 clouds. The traditional curve fittings to individual PDFs show that entrainment rate PDF can be fitted almost equally well with lognormal, gamma, and Weibull distributions, with most of R^2 larger than 0.90. A further analysis with the skewness–dispersion diagram shows that the Weibull distribution is the most appropriate for 5-m entrainment rate but the lognormal distribution is the most appropriate for cloud-mean entrainment rate.

For the parameters in lognormal distributions, μ increases with increasing mean relative humidity in the dry air and dilution ($1-LWC/LWC_a$); σ is weakly negatively correlated with relative humidity and $1-LWC/LWC_a$. For the parameters in gamma and Weibull distributions, both shape and scale parameters have positive correlations with relative humidity in dry air and dilution, respectively. Entrainment rate is negatively correlated with n , r_v , r_m , and LWC; positively correlated with ε ; and not significantly correlated with sd. Cloud droplet size distributions are significantly affected by entrainment rate. When entrainment rate is small, the distributions are stable, mainly between gamma and Weibull distributions. When entrainment rate is large, the distributions spread widely from Weibull distributions to gamma distributions, and to lognormal distributions. The variation in droplet size distributions with entrainment rate is generally consistent with the systems theory on the cloud droplet size distribution.

Acknowledgements This work was supported by the National Natural Science Foundation of China (41305120, 91337215); the Research Foundation for Environmental Protection of Jiangsu Province (2013042); the Natural Science Foundation of Jiangsu Province, China (BK20130988); the Specialized Research Foundation for the Doctoral Program of Higher Education (20133228120002); the Natural Science Foundation of the Higher Education Institutions of Jiangsu Province, China (13KJB170014); China Meteorological Administration Special Public Welfare Research Foundation (GYHY201406007); the Open Funding from State Key Laboratory of Severe Weather (2013LASW-B06); the Open Funding from Key Laboratory of Meteorological Disaster of Ministry of Education, China (KLME1305); the Qing Lan Project; a Project Funded by the Priority Academic Program Development of Jiangsu Higher Education Institutions; the US Department of Energy’s (DOE) Earth System Modeling (ESM) program via the FASTER project (www.bnl.gov/faster) and Atmospheric System Research (ASR) Program. Data used in this article are from the US Department of Energy ARM Aerial Facility’s RACORO Campaign. We appreciate the helpful discussions about the data with Drs. Andrew Vogelmann, Gunnar Senum, Seong Soo Yum, Haf Jonsson, Greg McFarquhar, and Hee-Jung Yang. We also appreciate Dr. Glenn Diskin’s help on the data from DLH.

Conflict of interest The authors declare that they have no conflict of interest.

References

1. Wang Z, Zhang H, Lu P (2014) Improvement of cloud microphysics in the aerosol-climate model BCC_AGCM2.0.1_CU-ACE/Aero, evaluation against observations, and updated aerosol indirect effect. *J Geophys Res* 119:8400–8417
2. Zhang H, Jing X, Li J (2014) Application and evaluation of a new radiation code under McICA scheme in BCC_AGCM2.0.1. *Geosci Model Dev* 7:737–754
3. Ma J, Guo X, Zhao C et al (2007) Recent progress in cloud physics research in China. *Adv Atmos Sci* 24:1121–1137
4. Lei H, Hong Y, Zhao Z et al (2008) Advances in cloud and precipitation physics and weather modification in recent years. *Chin J Atmos Sci* 32:967–974 (in Chinese)
5. Zhang D, Luo T, Liu D et al (2014) Spatial scales of altocumulus clouds observed with collocated CALIPSO and CloudSat measurements. *Atmos Res* 149:58–69
6. Zhang F, Li J (2013) Doubling–adding method for delta-four-stream spherical harmonic expansion approximation in radiative transfer parameterization. *J Atmos Sci* 70:3084–3101
7. Guo X, Fu D, Li X et al (2015) Advances in cloud physics and weather modification in China. *Adv Atmos Sci* 32:230–249
8. Lin Y, Zhao M, Ming Y et al (2013) Precipitation partitioning, tropical clouds, and intraseasonal variability in GFDL AM2. *J Clim* 26:5453–5466
9. Zhang GJ, Song X (2009) Interaction of deep and shallow convection is key to Madden–Julian Oscillation simulation. *Geophys Res Lett* 36:L09708
10. Wang Y, Zhou L, Hamilton K (2007) Effect of convective entrainment/detrainment on the simulation of the tropical precipitation diurnal cycle. *Mon Weather Rev* 135:567–585
11. Ping F, Gao S, Wang H (2003) Development and improvement of mass flux convection parameterization scheme and its applications in the seasonal climate prediction model. *Chin Sci Bull* 48:1006–1015
12. Huang Q, Yao S, Zhang Y (2009) Uncertainties of cumulus convective parameterization schemes over East Asia in RegCM3. In: 2009 sixth international conference on fuzzy systems and knowledge discovery. Tianjin, China

13. Wu T (2012) A mass–flux cumulus parameterization scheme for large-scale models: description and test with observations. *Clim Dyn* 38:725–744
14. Wang X, Zhang M (2014) Vertical velocity in shallow convection for different plume types. *J Adv Model Earth Syst* 6:478–489
15. Liu Y, Daum PH, Chai SK et al (2002) Cloud parameterizations, cloud physics, and their connections: an overview. *Recent Res Dev Geophys* 4:119–142
16. Xue H, Feingold G (2006) Large-eddy simulations of trade wind cumuli: Investigation of aerosol indirect effects. *J Atmos Sci* 63:1605–1622
17. Lu C, Liu Y, Niu S (2013) A method for distinguishing and linking turbulent entrainment mixing and collision-coalescence in stratocumulus clouds. *Chin Sci Bull* 58:545–551
18. Lu C, Liu Y, Niu S (2011) Examination of turbulent entrainment-mixing mechanisms using a combined approach. *J Geophys Res* 116:D20207
19. Stommel H (1947) Entrainment of air into a cumulus cloud. *J Meteorol* 4:91–94
20. Betts AK (1975) Parametric interpretation of trade-wind cumulus budget studies. *J Atmos Sci* 32:1934–1945
21. de Rooy WC, Siebesma AP (2008) A simple parameterization for detrainment in shallow cumulus. *Mon Weather Rev* 136:560–576
22. Del Genio AD, Wu J (2010) The role of entrainment in the diurnal cycle of continental convection. *J Clim* 23:2722–2738
23. Raga GB, Jensen JB, Baker MB (1990) Characteristics of cumulus band clouds off the coast of Hawaii. *J Atmos Sci* 47:338–356
24. Neggers RAJ, Duynkerke PG, Rodts SMA (2003) Shallow cumulus convection: a validation of large-eddy simulation against aircraft and Landsat observations. *Q J R Meteor Soc* 129:2671–2696
25. Gerber HE, Frick GM, Jensen JB et al (2008) Entrainment, mixing, and microphysics in trade-wind cumulus. *J Meteorol Soc Jpn* 86A:87–106
26. Jensen MP, Del Genio AD (2006) Factors limiting convective cloud-top height at the ARM Nauru Island climate research facility. *J Clim* 19:2105–2117
27. Wagner TJ, Turner DD, Berg LK et al (2013) Ground-based remote retrievals of cumulus entrainment rates. *J Atmos Ocean Tech* 30:1460–1471
28. Romps DM (2010) A direct measure of entrainment. *J Atmos Sci* 67:1908–1927
29. Dawe JT, Austin PH (2011) Interpolation of LES cloud surfaces for use in direct calculations of entrainment and detrainment. *Mon Weather Rev* 139:444–456
30. Dawe JT, Austin PH (2013) Direct entrainment and detrainment rate distributions of individual shallow cumulus clouds in an LES. *Atmos Chem Phys* 13:7795–7811
31. McCarthy J (1974) Field verification of the relationship between entrainment rate and cumulus cloud diameter. *J Atmos Sci* 31:1028–1039
32. de Rooy WC, Bechtold P, Fröhlich K et al (2013) Entrainment and detrainment in cumulus convection: an overview. *Q J R Meteor Soc* 139:1–19
33. Romps DM, Kuang Z (2010) Nature versus nurture in shallow convection. *J Atmos Sci* 67:1655–1666
34. Böing SJ, Jonker HJJ, Nawara WA et al (2013) On the deceiving aspects of mixing diagrams of deep cumulus convection. *J Atmos Sci* 71:56–68
35. Lu C, Liu Y, Niu S et al (2012) Lateral entrainment rate in shallow cumuli: dependence on dry air sources and probability density functions. *Geophys Res Lett* 39:L20812
36. Vogelmann AM, McFarquhar GM, Ogren JA et al (2012) RA-CORO extended-term aircraft observations of boundary layer clouds. *Bull Am Meteorol Soc* 93:861–878
37. Lu C, Liu Y, Niu S et al (2012) Observed impacts of vertical velocity on cloud microphysics and implications for aerosol indirect effects. *Geophys Res Lett* 39:L21808
38. Lu C, Liu Y, Niu S et al (2013) Empirical relationship between entrainment rate and microphysics in cumulus clouds. *Geophys Res Lett* 40:2333–2338
39. Zhang Q, Quan J, Tie X et al (2011) Impact of aerosol particles on cloud formation: aircraft measurements in China. *Atmos Environ* 45:665–672
40. Baumgardner D, Johnson H, Dawson W et al (2001) The cloud, aerosol and precipitation spectrometer: a new instrument for cloud investigations. *Atmos Res* 59–60:251–264
41. Diskin GS, Podolske JR, Sachse GW, et al (2002) Open-path airborne tunable diode laser hygrometer. In: *Proceedings of SPIE*. Seattle, WA, USA
42. Podolske JR, Sachse GW, Diskin GS (2003) Calibration and data retrieval algorithms for the NASA Langley/Ames diode laser hygrometer for the NASA transport and chemical evolution over the Pacific (TRACE-P) mission. *J Geophys Res* 108:8792
43. Lu C, Liu Y, Yum SS et al (2012) A new approach for estimating entrainment rate in cumulus clouds. *Geophys Res Lett* 39:L04802
44. Lehmann K, Siebert H, Shaw RA (2009) Homogeneous and inhomogeneous mixing in cumulus clouds: dependence on local turbulence structure. *J Atmos Sci* 66:3641–3659
45. Krueger SK (2008) Fine-scale modeling of entrainment and mixing of cloudy and clear air. In: *The 15th international conference on clouds and precipitation*. Cancun, Mexico
46. Lu C, Liu Y, Niu S et al (2013) Exploring parameterization for turbulent entrainment-mixing processes in clouds. *J Geophys Res* 118:185–194
47. Wang Y, Geerts B, French J (2009) Dynamics of the cumulus cloud margin: an observational study. *J Atmos Sci* 66:3660–3677
48. Guo X, Zheng G (2009) Advances in weather modification from 1997 to 2007 in China. *Adv Atmos Sci* 26:240–252
49. Hu Z, Lei H, Guo X et al (2007) Studies of the structure of a stratiform cloud and the physical processes of precipitation formation. *Chin J Atmos Sci* 31:425–439 (in Chinese)
50. Liu Y, Daum PH (2000) Which size distribution function to use for studies related to effective radius. In: *Proceedings of the 13th international conference on clouds and precipitation*. Reno, NV, US
51. Haman KE, Malinowski SP, Kurowski MJ et al (2007) Small scale mixing processes at the top of a marine stratocumulus—a case study. *Q J R Meteor Soc* 133:213–226
52. Lu C, Liu Y, Niu S (2014) Entrainment-mixing parameterization in shallow cumuli and effects of secondary mixing events. *Chin Sci Bull* 59:896–903
53. Liu Y (1995) On the generalized theory of atmospheric particle systems. *Adv Atmos Sci* 12:419–438
54. Liu Y, You L, Yang W et al (1995) On the size distribution of cloud droplets. *Atmos Res* 35:201–216
55. Liu Y (1997) On the unified theory of atmospheric particle systems part II: self-affine particles. *Adv Atmos Sci* 14:369–388
56. Liu Y, Hallett J (1997) The “1/3” power law between effective radius and liquid-water content. *Q J R Meteor Soc* 123:1789–1795
57. Liu Y, Hallett J (1998) On size distributions of cloud droplets growing by condensation: a new conceptual model. *J Atmos Sci* 55:527–536
58. Liu Y, Daum PH, Hallett J (2002) A generalized systems theory for the effect of varying fluctuations on cloud droplet size distributions. *J Atmos Sci* 59:2279–2290

After acceptance

My Publication

Upon acceptance of your article you will receive a link to the special Author Query Application at Springer's web page where you can sign the Copyright Transfer Statement online and indicate whether you wish to order Open Choice, offprints, or printing of figures in color. A Springer Open Choice article receives all the benefits of a regular subscription-based article, but in addition is made available publicly through Springer's online platform SpringerLink. Once the Author Query Application has been completed, your article will be processed and you will receive the proofs.

Copyright transfer

Authors will be asked to transfer copyright of the article to the Publisher (or grant the Publisher exclusive publication and dissemination rights). This will ensure the widest possible protection and dissemination of information under copyright laws.

Open Choice articles do not require transfer of copyright as the copyright remains with the author. In opting for open access, the author(s) agree to publish the article under the Creative Commons Attribution License.

Language

Manuscripts that are accepted for publication will be checked by our copyeditors for spelling and format style. This may not be sufficient if English is not your native language and substantial editing would be required. In that case, you may want to ask a native speaker to help you or arrange for your manuscript to be checked by a professional language editor prior to submission. A clear and concise language will help editors and reviewers concentrate on the scientific content of your paper and thus smooth the peer review process.

Use of an editing service is neither a requirement nor a guarantee of acceptance for publication.

Proof reading

The purpose of the proof is to check for typesetting or conversion errors and the completeness and accuracy of the text, tables and figures. Substantial changes in content, e.g., new results, corrected values, title and authorship, are not allowed without the approval of the Editor.

After online publication, further changes can only be made in the form of an Erratum, which will be hyperlinked to the article.

Page charges and offprints

Page charges are 300 RMB (US \$50) for each page in black and white and 1000 RMB (US \$200) for each color page. An invoice will be sent to the corresponding author by the Editorial Office. If offprints and sample journals are required, please contact the managing editor and pay extra fee. The full text article opens free to the readers inside China at <http://www.scibull.com:8080/EN/volumn/home.shtml>, and the full text in English is available to overseas readers at <http://link.springer.com/journal/11434>

Online first

The article will be published online after receipt of the corrected proofs. This is the official first publication citable with the DOI. After release of the printed version, the paper can also be cited by issue and page numbers.



Articles | Reviews | Letters | News & Views | Research Highlights | Comments | Correspondences | etc.

High impact—a semi-monthly multidisciplinary journal co-sponsored by the Chinese Academy of Sciences and the National Natural Science Foundation of China

Broad coverage—reports on significant advances across a broad range of natural sciences and engineering fields around the globe

Rapid publication—a fast-paced platform for cutting-edge research findings, insightful reviews and news, and discussions of upcoming trends relevant to science and scientists

- Indexed by SCI, CA, etc.
- Online First Publication
- Open Choice

ISSN 2095-9273



9 772095 927159